Sensitivity of Tropical Convection to Sea Surface Temperature in the Absence of Large-Scale Flow

ADRIAN M. TOMPKINS* AND GEORGE C. CRAIG

JCMM, Department of Meteorology, University of Reading, Reading, United Kingdom

(Manuscript received 5 September 1997, in final form 12 February 1998)

ABSTRACT

The response of convection to changing sea surface temperature (SST) in the absence of large-scale flow is examined, using a three-dimensional cloud resolving model. The model includes a five-category bulk microphysical scheme representing snow, ice, graupel, rain, and cloud amounts in addition to an interactive radiation scheme for the shortwave and infrared. Long integrations are made to achieve a radiative–convective equilibrium state for SSTs of 298, 300, and 302 K, for which cloud and convection statistics are analyzed.

The main conclusion of the paper is that, despite significant temperature sensitivities in many of the conversion terms between bulk water categories, convection is very insensitive to changing SST in the absence of large-scale flow. This is a result of the moist adiabatic temperature profile that the tropical atmosphere is constrained to take. A parcel of air rising through a deep convective cloud experiences approximately the same range of temperatures but at higher altitudes as SST increases. Thus the vertical profiles of cloud fraction and other cloud-related statistics are simply shifted in height, but not changed in overall magnitude.

The small changes in cloud properties that do occur lead to a small reduction in cloud fraction as SST increases. This appears to be due to an increase in graupel amounts with respect to snow, giving smaller cloud fractions since graupel has a higher fall velocity. The radiative effects of the changes in atmospheric properties are examined and it is found that the model atmosphere exhibits no supergreenhouse effect since atmospheric relative humidity is not altered significantly by the SST changes. The water vapor feedback effect is largely canceled by the change in temperature. Clouds have a negligibly small, but highly nonlinear, feedback in the model climate, in the absence of large-scale flow.

1. Introduction

In climate research, the actions of water vapor and clouds are considered to be crucial factors in our prediction of possible future climates because of their possible ability to amplify or reduce any potential warming due to increasing greenhouse gas amounts, but according to the latest Intergovernmental Panel on Climate Change (IPCC) report the water vapor feedback is still a ''substantial uncertainty'' and cloud feedback is a ''major source of uncertainty'' (Dickinson et al. 1996). In the Tropics the two effects are inextricable tied since convective activity is the main source of water vapor in the free troposphere (Betts 1990; Sun and Lindzen 1993). Thus an understanding of the control of convection is essential if we are to understand cloud and vapor feedbacks in the Tropics. Over the past three decades, however, efforts to understand convection have largely been motivated by the requirement to parameterize its effect in atmospheric general circulation models (GCMs), which must use grid sizes too coarse to explicitly resolve convective motions. This has naturally lead to a view of convection influenced by local-scale atmospheric thermodynamic properties, determined largely by the local sea surface temperature (SST), and so-called large-scale motions, which are essentially the atmospheric motions resolved by the GCM grid. In some cases (e.g., Kuo 1974; Tiedtke 1989) the control of convection depended explicitly on the large-scale motion. Thus to examine the question of how local properties or large-scale motion affect convection it is not realistic to use GCM experiments that contain such in-built assumptions.

A number of observational studies have examined the relationship between convective activity and local SST (e.g., Graham and Barnett 1987; Ramanathan and Collins 1991; Waliser and Graham 1993; Zhang 1993; Arking and Ziskin 1994; Fu et al. 1994), and despite some differences in their conclusions the general observation was one of a drastically increasing occurrence of deep convection above a ''critical SST'' ranging from 26° to 27°C, with a large variability especially observed at

* Current affiliation: Max-Planck-Institut für Meteorologie, Hamburg, Germany.

Corresponding author address: A. M. Tompkins, Max-Planck-Institut für Meteorologie, Bundesstrasse 55, 20146 Hamburg, Germany. E-mail: Tompkins@dkrz.de

higher SSTs. As noted in many of these studies, one possible reason for this large variability is that the observations are taken from a wide range of atmospheric dynamical conditions, ranging from highly suppressed circumstances to region of substantial mean upward motion. A recent study of Lau et al. (1997) highlighted the difficulty in unambiguously isolating one effect (large-scale flow) from two others (changing SST and convective activity) when a three-way coupling exists. They used conditional sampling to remove the effects of the large-scale flow from an observational dataset to obtain a purely thermodynamic relationship between convection and sea surface temperature. They found that the sensitivity of convection to SST was greatly reduced when the large-scale flow effects were removed. In their conclusions Lau et al. (1997) state that the limited sensitivity to local thermodynamic properties could be further reduced if higher resolution data than monthly averages were to be used, and conclude that ''Clearly the results . . . should be tested with numerical models.'' Bony et al. (1997) used the same technique to examine the influences of SST and large-scale motion on the tropical greenhouse effect and cloud radiative forcing and showed that the critical SST at which deep convection begins to occur is indeed directly linked to the occurrence of large-scale upward atmospheric motion.

Increasing computer resources now allow the cloud resolving model (CRM), which explicitly resolves cloud-scale dynamics, to be used in a new way to test these ideas by permitting the long integration times necessary to achieve a full radiative–convective equilibrium. Using these models, the physical processes of convective-scale dynamics, surface fluxes, and radiative heating rates and their interactions are explicitly represented. Previous CRM studies of radiative–convective equilibrium have been conducted by Held et al. (1993), Lau et al. (1993), Sui et al. (1994), Grabowski et al. (1996), and Xu and Randall (1997). In particular, two studies have focused on the question of convective sensitivity to SST and large-scale convergence, namely those of Sui et al. (1993) and Lau et al. (1994). In their studies a CRM model was operated to equilibrium over an SST of 28°C followed by two sensitivity studies in which a large-scale forcing was first applied, followed by an experiment with an increased SST of 30°C. One of their main findings was that the sensitivity to large-scale motions was far greater than the sensitivity to underlying SST, consistent with the observational results of Lau et al. (1997).

All of the above CRM investigations have a factor in common in that they were conducted using a two-dimensional (2D) domain. However, some sensitivity studies conducted by Tompkins (1997) indicated that significant differences in cloud and convective properties can occur between two- and three-dimensional (3D) geometry. Recently Tompkins and Craig (1998a, hereafter TC98a) have integrated a 3D cloud model to a radiative–convective equilibrium state. The model included a microphysical scheme that represented ice, snow, graupel, rain, and cloud amounts with prognostic equations, a fully interactive radiative scheme for the calculation of infrared and shortwave atmospheric heating rates, and a wind sensitive surface flux formulation. Imposing a fixed underlying SST of 300 K but no large-scale forcing, the model reached an equilibrium with profiles not unlike those of the tropical mid-Pacific. Thus this model represents a tool with which the effect of differing thermodynamic conditions on convection can be studied, in which convective-scale interactions are represented and where no effects of large-scale flow are included.

This study aims to follow on from TC97a and gain a better understanding of the origin of thermodynamic insensitivity of convective properties such as anvil coverage and cloud microphysical processes by analyzing the sensitivity of the model equilibrium state to changes in underlying SST. The details of the experimental setup are summarized in section 2. Section 3 shows that an equilibrium climate is achieved in each experiment, and sections 4 and 5 give some general statistics of the equilibrium states. Section 6 examines the sensitivity of the microphysical processes. By examining the radiative fluxes at the top of the model atmosphere it is possible to calculate a local tropical feedback factor for clouds, water vapor, and temperature lapse rate (e.g., the effect that these quantities would have in amplifying or decreasing the atmosphere's response to a greenhouse warming), which is accomplished in section 7.

2. Experiment details

a. Model description

Only brief details will be given here since a detailed model description is contained in Shutts and Gray (1994) and TC98a. The basic cloud model is anelastic with an advanced total variation diminishing scheme for advection of all prognostic quantities (Leonard 1991). The microphysical scheme, a slightly modified version of that used in TC98a, integrates prognostic equations for rain, snow, cloud water, cloud ice, and graupel amounts (Swann 1994; Brown and Swann 1997). In the microphysical scheme only the categories of snow, graupel, and rain are assumed to have a nonzero fall speeds.

The radiation scheme that has been added to the model calculates heating rates for both the shortwave and infrared spectrums dividing the former into nine bands and the latter into six. It is based on the two-stream approximation and is outlined in Edwards and Slingo (1996) and tested against observations in Taylor et al. (1996). The scheme takes the mixing ratios of the microphysical quantities into account when calculating heating rates. These mixing ratios also alter the effective radii of the water categories, following Petch (1998). The radiation scheme is called every 120 time steps, which is equivalent to an average of every 16 min. This

TABLE 1. Experimental setup.

Domain size (x, y, z)	60 km × 60 km × 21 km
Horizontal resolution	2 km
Number of vertical levels	35
Vertical resolution	Stretched grid: 130 m at surface 950 m in upper troposphere
Boundary conditions	Lateral periodic Fixed lid Zero slip for surface flux calculation
Large-scale forcing	Radiation only

is shorter than the cumulus timescale in an attempt to eliminate ''ghost clouds'' in the forcing. The absence of a background mean wind means that convective clouds are not advected horizontally significantly during their lifetime, allowing a longer ''radiation time step'' than that suggested by Xu and Randall (1995). However, cloud–radiation interactions at the cloud-top boundary will be poorly represented, although to correctly represent these a much higher vertical resolution would also be necessary (Petch 1995). The solar zenith angle is fixed at 51.7° to ensure a realistic path length, with an appropriate ''length of day'' factor utilized to make the solar constant 685 W m^{-2}. The surface fluxes of water vapor and heat are calculated using a formulation based on Monin–Obukhov theory based on Eqs. (3.23), (3.24), (3.29), and (3.33) of Garratt (1992) with constants given in TC98a. The use of this formulation makes it unnecessary to impose a minimum surface wind speed, which is necessary to produce realistic fluxes in low wind conditions if a bulk aerodynamic formula is used.

b. Experiment design

The experimental setup is summarized in Table 1. The horizontal domain size was used for these experiments of 60 km × 60 km, and 21 km in the vertical. This domain size is large enough to almost continuously include at least one deep convective event throughout the integration (in addition to more common shallow convective activity), with only short occasional periods with no active convection.

The horizontal resolution is chosen to marginally resolve deep convection at 2 km and represents the finest resolution that could be applied with the available computing resources. Short sensitivity tests with the cloud-resolving model using a higher resolution indicated that the deep convective cells were usually on the scale of around 2 km but indicated that shallow convection could be under resolved. The vertical grid consists of 35 levels, with a Newtonian sponge layer applied to the top 6 layers above 16.3 km. The first model half level is set at 50 m above the surface, with Δz ranging from 130 m at the surface to approximately 1 km at the top of the domain. The vertical velocity is set to zero at the bottom and top of the domain and the lateral boundary conditions imposed are cyclic. There is no imposed convergence into the domain, no forced uplift, no imposed wind shear, and no rotation.

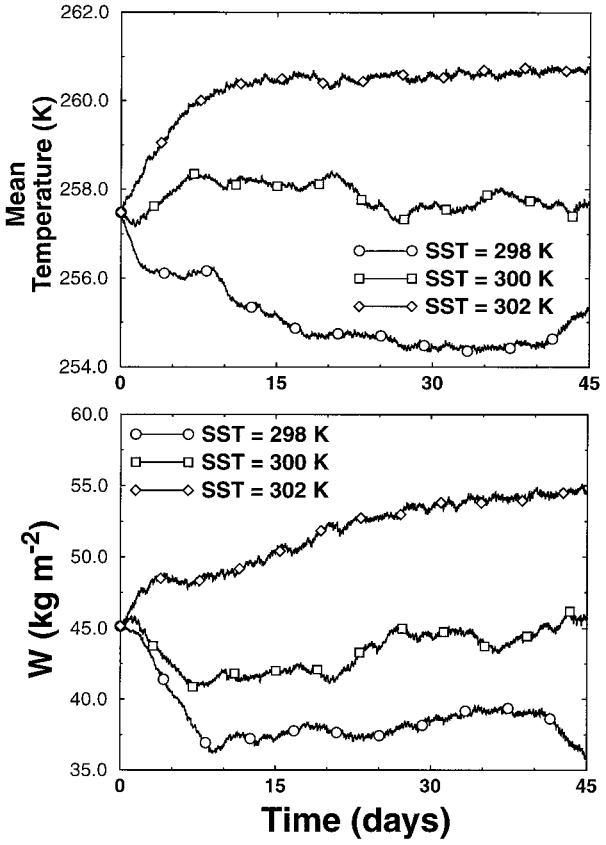

FIG. 1. Time series of domain mean temperature and atmospheric precipitable water (W) for the three SST experiments.

The model was initialized from a resting state with an underlying SST of 300 K and atmospheric temperature and moisture profiles taken from the equilibrium run of TC98a. The model was integrated for one day to establish a realistic cloud field, at which point three model integrations were initiated: in the first the SST remained at 300 K and in the second and third the SST was changed to 298 and 302 K, respectively (sometimes referred to as the ''cold'' and ''warm'' runs). All three runs were integrated for a period of 45 days.

3. Adjustment to equilibrium

In order to plot the adjustment to equilibrium, Fig. 1 shows the evolution of the domain mean temperature and total column water vapor (precipitable water) starting at the point at which the SST perturbations were applied. A general adjustment to the new equilibrium values occurs over the 45-day period, which is superimposed by significant oscillations of periods of up to several days that were also apparent in TC98a. These shorter-term oscillations render it more difficult to es-

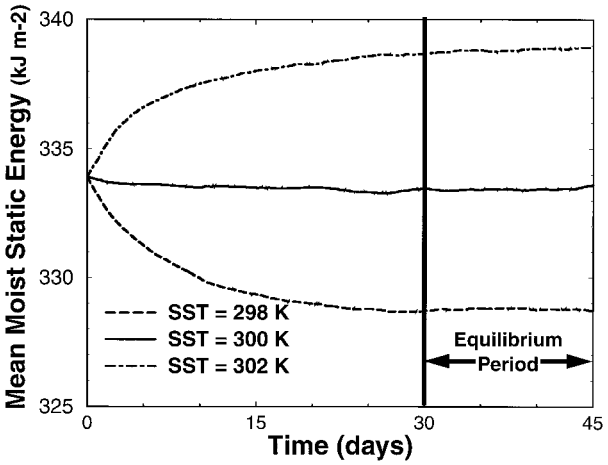

FIG. 2. Time series of mean moist static energy for the three SST experiments.

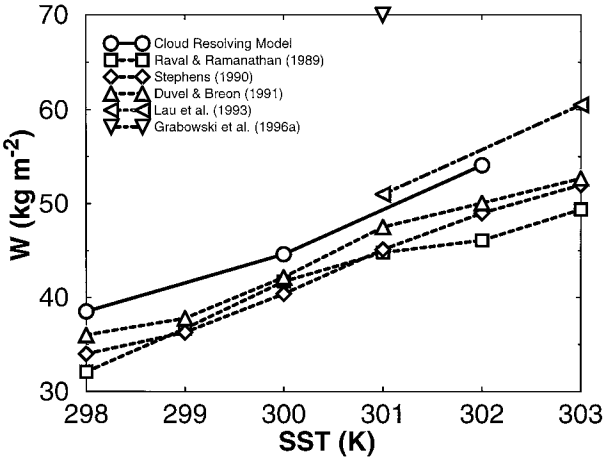

FIG. 3. Atmospheric water vapor amount as a function of SST.

tablish the point in time at which equilibrium is achieved. However, in a study of convective adjustment timescales, Tompkins and Craig (1998b) indicated that to reveal the adjustment to equilibrium most clearly the domain mean moist static energy should be analyzed, since this quantity is not affected by convective overturning of the atmosphere and therefore exhibits no short-term variability. The moist static energy for the three runs is shown in Fig. 2 and the long-term exponential trend to equilibrium is clear. There is a small difference in equilibrium states between the control run here and the experiment of TC98a due to the modifications in model setup and physics. It is clear that all three experiments have reached equilibrium status by day 30, and thus the period from day 30 to 45 is referred to as the ''equilibrium state'' throughout the remainder of this work.

4. Domain mean properties

a. Column integrated water vapor

One of the quantities that is difficult for a CRM (or indeed any model) to predict in a long-term simulation is the atmospheric water vapor profile (Emanuel 1996). One difficulty is that in the Tropics convective activity, and therefore cloud-scale microphysical processes, largely determine the atmospheric vapor profile (Betts 1990; Sun and Lindzen 1993), and these microphysical processes are some of the least known parameterizations contained in CRMs. In their long-term CRM study in which Global Atmospheric Research Program Atlantic Tropical Experiment data was used to force convection in a 2D CRM, Grabowski et al. (1996) found mid- and upper-troposphere moisture values tended to be too high by 10%–20%. Shine and Sinha (1991) showed that the radiative importance of water vapor changes is roughly proportional to the fractional change and so small absolute changes in the upper troposphere can be radiatively important.

Observational satellite data reveals some information concerning the vertical structure of moisture in the Tropics, but to date studies examining relationships to SST have mostly considered column integrated water vapor (W; Raval and Ramanathan 1989; Stephens 1990; Duvel and Bréon 1991). Gaffen et al. (1992) examined the water vapor–SST relationship using radiosonde data and found a good agreement with these satellite studies over warm oceans. The CRM's water vapor amount is compared to the satellite studies and two previous 2D CRM studies in Fig. 3 and it is seen that the 3D CRM has an equilibrium value of W that agrees closely with observations, although the model atmosphere is a little too moist. Such comparisons with observations must be made with caution however, since the effect of the large-scale flow is present in observational data, as discussed in the introduction. The 2D CRM study of Lau et al. (1993) also has a similar sensitivity of W to observations but is slightly moister. Grabowski et al. (1996) achieved a much wetter atmosphere. Xu and Randall (1997) applied different set large-scale forcings in their CRM experiments and achieved moisture values that ranged between the results of the latter two studies.

b. Cloud fraction

Satellite data has also been used in recent years to reveal much information about cloud properties (e.g., Ramanathan et al. 1989; Ramanathan and Collins 1991). One important property is the fractional cloud coverage, since the amount of shortwave radiation reflected back to space is strongly dependent on it. To calculate the cloud fraction in the cloud model, the cloud, ice, snow, and graupel mixing ratios are summed at each grid point, which is classified as cloudy if this amount exceeds 0.005 g kg^{-1} (as in TC98a except that rain is neglected here). Any column is defined as cloudy if it contains at

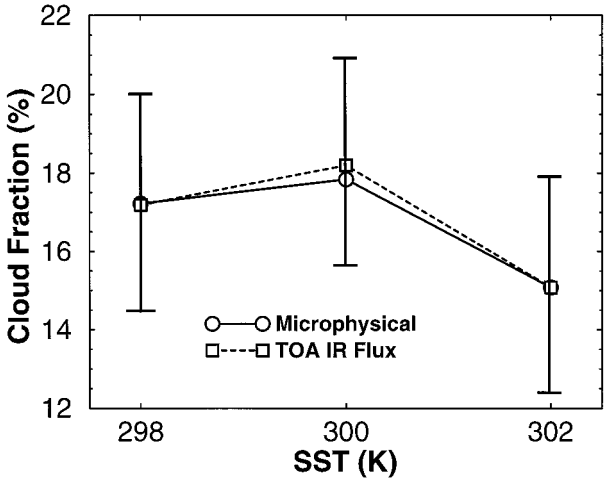

FIG. 4. Domain cloud fraction as a function of SST, calculated using the TOA IR flux and the column amount of condensates. The vertical lines indicate the standard deviation of the cloud amount calculated from the IR TOA flux.

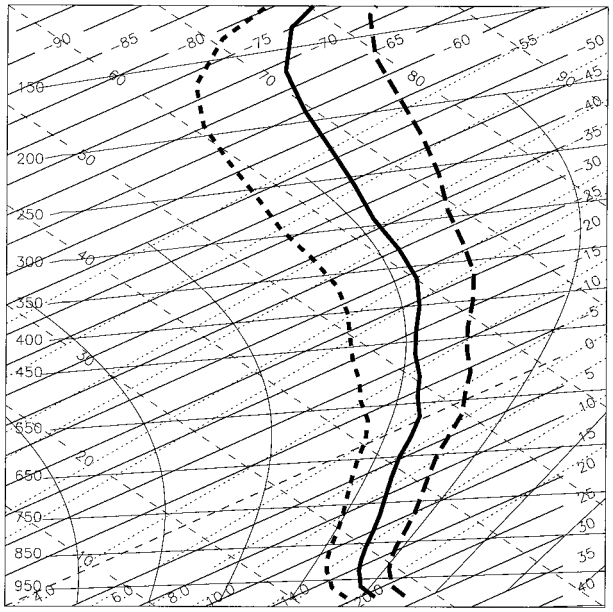

FIG. 5. Domain mean temperature profile for the three equilibrium states with SST = 298 K (short dash), 300 K (solid), and 302 K (long dash).

least one cloudy grid point. A estimate of cloud fraction is also made using the infrared (IR) top of the atmosphere (TOA) fluxes, where a brightness temperature of less than 270 K defines a column as cloudy. This is very close to the threshold suggested by Fu et al. (1990) of 267 K and the same as that used by Zhang (1993), who stated the choice was somewhat arbitrary. The cloud-fraction estimate is fairly insensitive to the threshold used in all three cases due to the fact that the cloud boundaries are sharply defined.

Cloud fraction in the cloud resolving model is found to be quite insensitive to changes in SST (Fig. 4) and the methods of calculating cloud fraction are seen to agree well. The actual figures ranging from 14% to 18% are somewhat smaller than the observed values derived using the TIROS Operational Vertical Sounder dataset (approximately 20%–30%) and substantially smaller than those derived from the ISCCP dataset (approximately 55%–65%) taken from a similar dynamical regime and SST range (Bony et al. 1997). Perhaps surprisingly, the cloud fraction actually drops slightly with SST for the SST = 302 K run. Although there is of course much temporal variability in cloud-fraction amounts, shown by the large standard deviations of the cloud cover figures in the plot, these features are found to be robust for any 10-day averaged period during the last 25 days of the experiments and will be examined further in the following section. With large-scale motion effects removed, Bony et al. (1997) also found cloud fraction to be relatively insensitive to SST in this range compared to the mean cloud fraction calculated across all dynamical regimes.

5. Vertical structure of equilibrium states

a. Temperature structure

A convenient way to examine temperature is to use a tephigram since this allows easy comparison to the moist adiabatic profile that the temperature in the Tropics is often assumed to approximate. Figure 5 shows that the temperature profile in each case does resemble a moist adiabat above the dry adiabatic boundary layer. This implies that the largest temperature changes occur in the upper troposphere, which in turn means that the potential temperature lapse rate is increasing with SST. There is a boundary layer that is well mixed in potential temperature, which appears to remain approximately constant in height, although small changes are not possible since the layer is represented by only three model gridpoints. The temperature response appears to be approximately linear throughout the troposphere.

b. Relative humidity

Since water vapor has a vertical-scale height of around 2 km the column-integrated water amounts shown earlier could hide significant changes in upper-tropospheric water vapor that could be proportionally far greater or less than the change in the column-integrated water amount. As stated previously, the radiative response to water vapor is sensitive to fractional rather than absolute changes. Although it is generally accepted that mixed-layer atmospheric relative humidities in the Tropics are fairly constant with temperature it is currently not clear how the free troposphere above will respond to external forcings, in particular at high level near the region of detrainment from deep convection. Figure 6 plots the relative humidity in the three equilibrium states and shows that it remains roughly unchanged in all three experiments below 9 km, the dif-

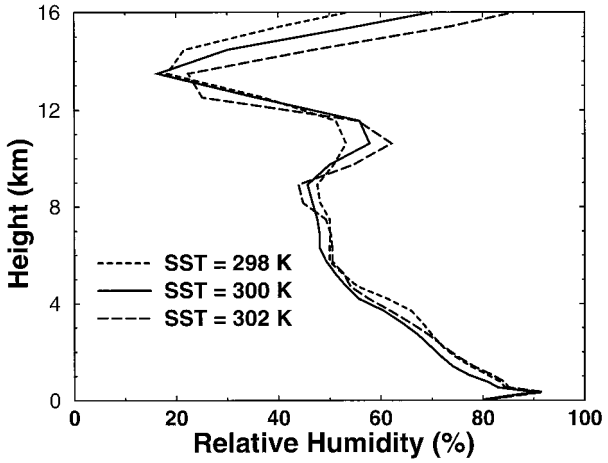

FIG. 6. Vertical profiles of relative humidity for the three equilibrium states. Above the freezing level, relative humidity is calculated with respect to ice saturation.

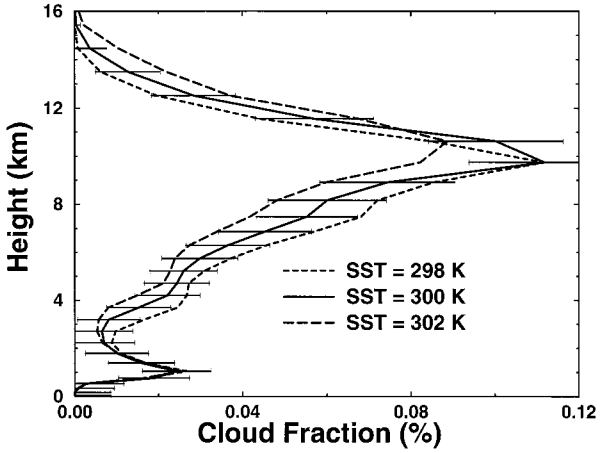

FIG. 7. Vertical profile of cloud fraction for the three equilibrium states. The horizontal bars represent the standard deviation of the cloud fraction in the control run.

ferences between the three cases being less than the standard deviation. Only at the deep convective detrainment level at around 10 to 12 km is there a significant trend, with a progressive decrease in relative humidity with SST.

c. Cloud fraction

In the previous section the domain cloud fraction was seen to reduce slightly with increasing SST. To give a clearer picture as to how the cloud behavior changes, Fig. 7 shows the cloud fraction as a function of height. The cloud-fraction profile in all SST experiments exhibits a low-level peak in cloud fraction at around 1 km corresponding to shallow convection and a steady increase from 3 km to the deep convective cloud detrainment level at around 10 km in altitude. The overall impression is that as SST increases the cloud profile is moved upward in height, so that below the deep convective detrainment level at any given height the cloud fraction falls with increasing SST whereas an increase in cloudy fraction is apparent above this level. For example the cloud fraction at 8 km drops from a little over 7% to around 4.5% when the SST increases from 298 to 302 K, whereas an increase from 3.3% to 5.3% occurs at 12 km. The peak in cloudy fraction is around 11% for SST = 298 and 300 K, which drops to 9% for SST = 302 K. This reflects the cloud fraction figures in the previous section that are dominated by anvil cloud coverage. As stated earlier, cloud fraction exhibits significant variability, but the differences between the cold and the warm run are generally greater than the standard deviation of the cloud amount throughout the free troposphere. The shallow convective boundary layer cloud remains virtually unchanged in all three cases.

In order to estimate the change in detrainment height from deep convection the height of neutral buoyancy was examined again assuming reversible moist adiabatic parcel ascent from the 50-m level for the equilibrium mean profile. This gave predicted cloud-top heights of 12.5, 12.9, and 13.1 km as SST increases, which agrees reasonably well with cloud-top heights calculated from instantaneous cloud fields that changed from around 11.6 to 12.5 km across the SST range but of course is severely constrained by model resolution (the next model grid level above these two being situated at 13.5 km). The height of the peak in the cloud fraction was calculated by fitting cubic spline curves to the profiles in Fig. 7, and it was found that the peak cloudiness occurred at 9.8, 10.0, and 10.4 km, respectively. This is lower than the calculated neutral buoyancy since clouds do not detrain exactly at the neutral buoyancy level but instead detrain across a range of heights for which the in-cloud buoyancy is falling with height (Bretherton and Smolarkiewicz 1989) However, the predicted cloud height increase of 600 m seems to be a reasonable estimate.

d. Convective mass flux

The convective transport of water vapor in response to the SST can be altered because of changing kinematic properties of convection, in addition to temperature sensitive microphysical processes that alter the distribution of falling condensates. However, one would expect a vast change in net convective mass flux in these experiments since it is constrained to balance the clear-sky radiative cooling (Emanuel et al. 1994). Thus only large alterations in clear temperature and water vapor amounts could feed back to substantially alter convective mass fluxes.

To examine the up and downdraught convective mass fluxes it is necessary to provide a method for identifying convective grid points and here the kinematic threshold of an absolute vertical velocity exceeding 1 m s^{-1} is used. This is a commonly used criteria for identifying

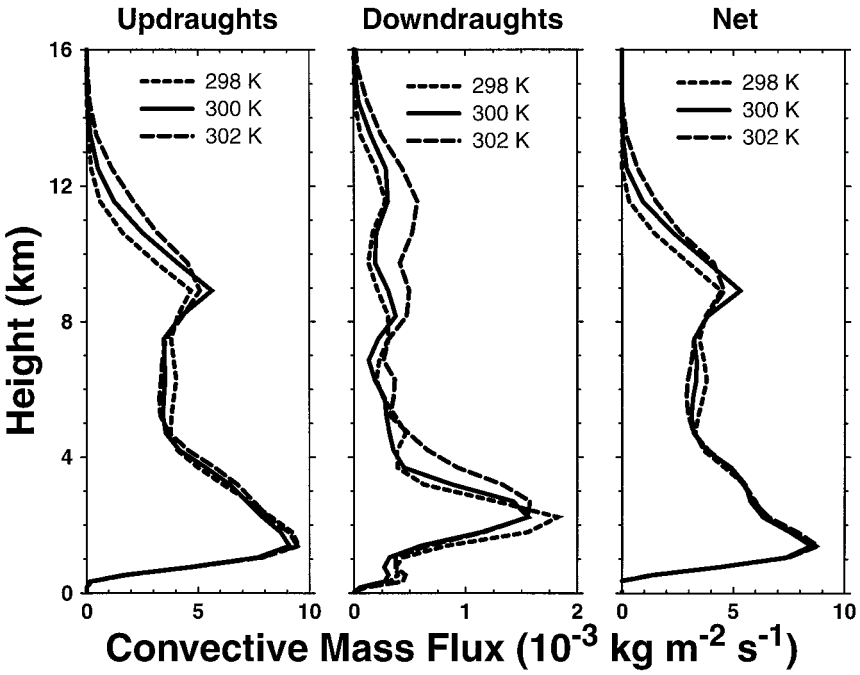

FIG. 8. Updraft, downdraft, and net convective mass flux for the three equilibrium states.

convective cores (e.g., Lemone and Zipser 1980; Jorgensen and Lemone 1989; Lucas et al. 1994; Robe and Emanuel 1996), although it may be argued that since downdraft core velocities are smaller than in their updraft cousins, a correspondingly smaller threshold for their identification should be used. It is seen that overall there is very little change in the updraft mass flux (Fig. 8). In the lower 4 km of the atmosphere the changes are almost imperceptible, consistent with the unchanging cloud fraction at these levels. In the model upper levels the mass flux increases, as one would expect if the convective towers are reaching higher altitudes. The second panel of Fig. 8 shows the downdraft mass flux, which exhibits a markedly different behavior. The change with SST appears very nonuniform with little difference to be identified between the SST = 298 K and SST = 300 K experiments but increases in the SST = 302 K run throughout the troposphere above 3 km, which amounts to a doubling of mass flux above 8 km. In these experiments, where the absence of strong vertical wind shear leads to upright convection, the downdraft mass fluxes are relatively small and the net mass flux largely reflects the behavior observed for the updrafts.

6. Microphysics

The insensitivity of relative humidity and cloud fraction to SST observed in the previous two sections is perhaps surprising given the extreme temperature sensitivity of many cloud microphysical processes. Since the microphysical scheme contains 37 conversion terms for the conversion between the various water categories, it is beyond the scope of this paper to give a detailed analysis of the temperature sensitivity of each of these equations and instead a brief examination of the warm-phase and ice-phase microphysics is made in turn.

a. Warm rain microphysics

As SST increases over the tropical oceans, one would expect an increasing dominance of warm–cloud microphysical processes, since the depth of the atmospheric layer with temperatures exceeding the freezing point of water must increase. To examine this in the cloud-model experiments, Fig. 9 shows the conversion rates due to the warm rain microphysical processes of the autoconversion of cloud drops to form rain, the collection of cloud water by falling raindrops, and the evaporation of raindrops to give water vapor. The autoconversion graphs shows a double peak structure with an increase in cloud water apparent above the freezing level for around 1.5 km in each case. The fact that liquid cloud can be formed above the freezing level is a consequence of the model assumption that no supersaturation with respect to water vapor can exist, but that ice formation and growth takes a finite time. Thus in strong updraft cores it is possible that large enough supersaturations with respect to ice can exist, so that liquid cloud is assumed to immediately form, which is subsequently converted to raindrops. This is consistent with observations that cumulus clouds frequently contain supercooled liquid droplets.

As expected, an examination of the conversion rates

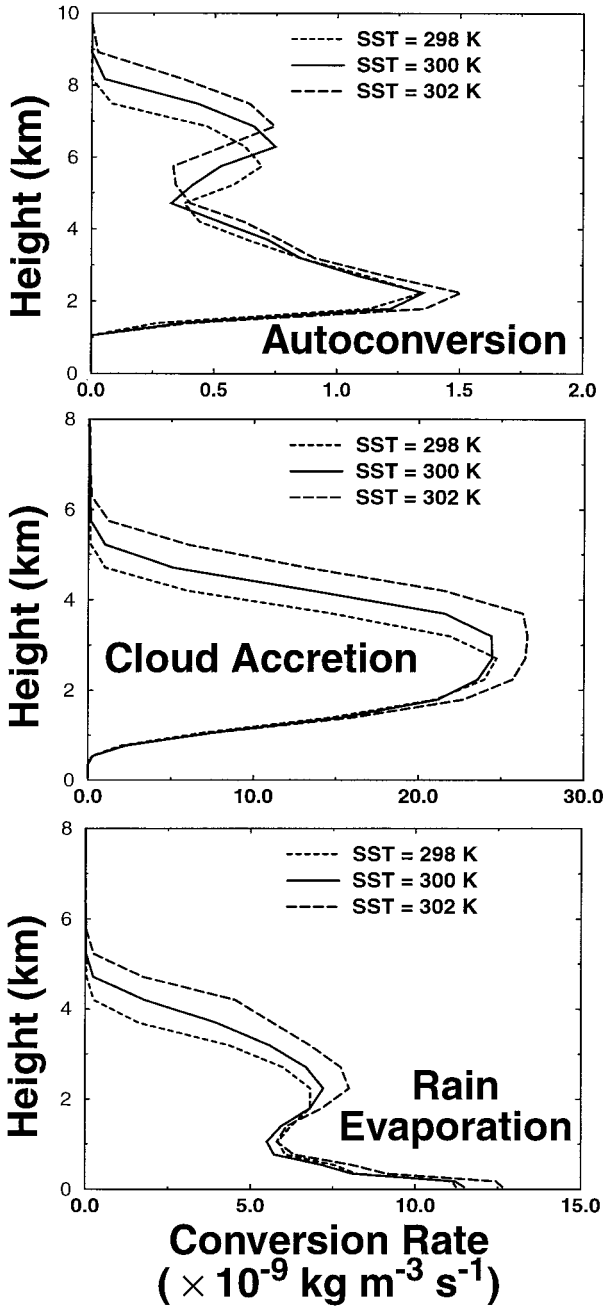

FIG. 9. Plots of the warm microphysical cloud processes of (top) autoconversion of cloud water to rain, (middle) collection of cloud water by rain, and (bottom) evaporation of raindrops for the three equilibrium experiments.

in Fig. 9 reveals the deepening of the warm rain microphysical layer, and in particular it shows limited increases in magnitude of the conversion rates for the warm SST case, which follows from the moister atmosphere. Given these changes it is perhaps somewhat surprising that the equilibrium relative humidity profile is so insensitive to changes in underlying surface temperature. For example, one might expect that higher production of rain would lead to a moister atmosphere due to the increased evaporation rates as rain falls through a subsaturated environment. One reason for this relative insensitivity could be the upright nature of the convection in these simulations, so that the warm rain microphysical processes are restricted to the convective cores and the intense low-level downdrafts that develop directly below them.

b. Ice-phase microphysics

To simplify the analysis of the ice-phase microphysical processes, the total sources and sinks for each of the ice-water categories are summed for the cold and warm runs (Fig. 10), which reveal the broad tendencies that one expects. For example, ice is created in a band starting immediately above the melting layer as the initial small ice crystals are created in the convective updrafts, whereas the sink for ice peaks at the detrainment level as ice is converted to the categories of snow and graupel within the anvils or simply evaporates on mixing with the subsaturated cloud environment. The snow sink term exhibits a double peak structure that is contributed to by three microphysical processes. The peak aloft is due to the autoconversion of snow into graupel, and the peak at around 7–8 km divides almost equally into the collection of snow by graupel and the sublimation of snow to water vapor. Presumably, collection of snow occurs mostly within the upright convective cores, whereas sublimation occurs outside the towers as the high-level downdrafts (identified by TC98a, that result directly from the high-level cloud outflow) mix with subsaturated air. The conversion rates for graupel are larger than for the other categories since a considerable amount of water vapor accretion is involved.

The important aspect of this figure, though, is that despite the fact that many of the conversion parameterizations are very sensitive to temperature (with more than order of magnitude changes in conversion rates expected at any certain height between these two runs), the overall profiles hardly alter in magnitude at all. Instead the profiles are simple shifted upward as the atmospheric temperature warms. This behavior is a result of the moist-adiabatic temperature profile the tropical atmosphere is constrained to adhere to. Although the temperature sensitive microphysical exchange rates can vary considerably at a fixed height as the atmospheric temperature changes with SST, a parcel undergoing ascent through a deep convective cloud feels approximately the same range of temperatures, simply at a different altitude. While the temperatures are encountered at a different altitude, the microphysical conversions are not sensitive to pressure except in the calculation of saturation over ice or water. The result is apparently a simple upward displacement of the microphysical conversions, without significant changes in the relative humidity.

To examine the changing balance in microphysics

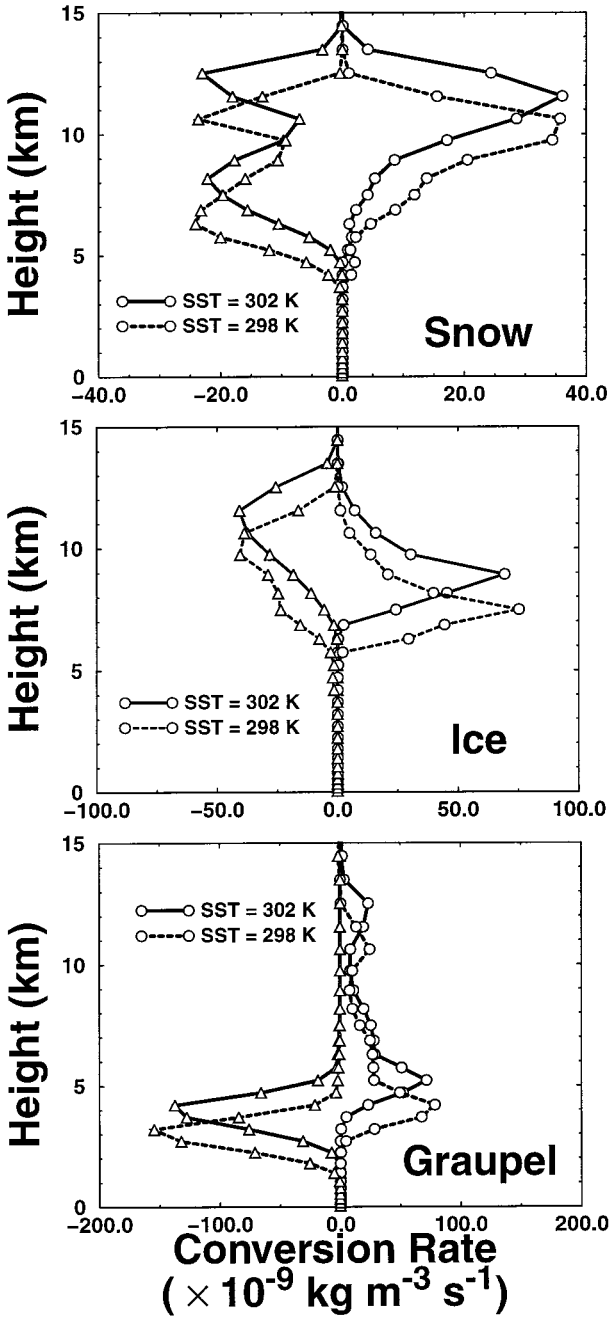

FIG. 10. Total source–sinks of the ice microphysical quantities of (top) snow, (middle) ice, and (bottom) graupel for the SST = 298 K and SST = 302 K experiments. The profile for the SST = 300 K run lies halfway between the two.

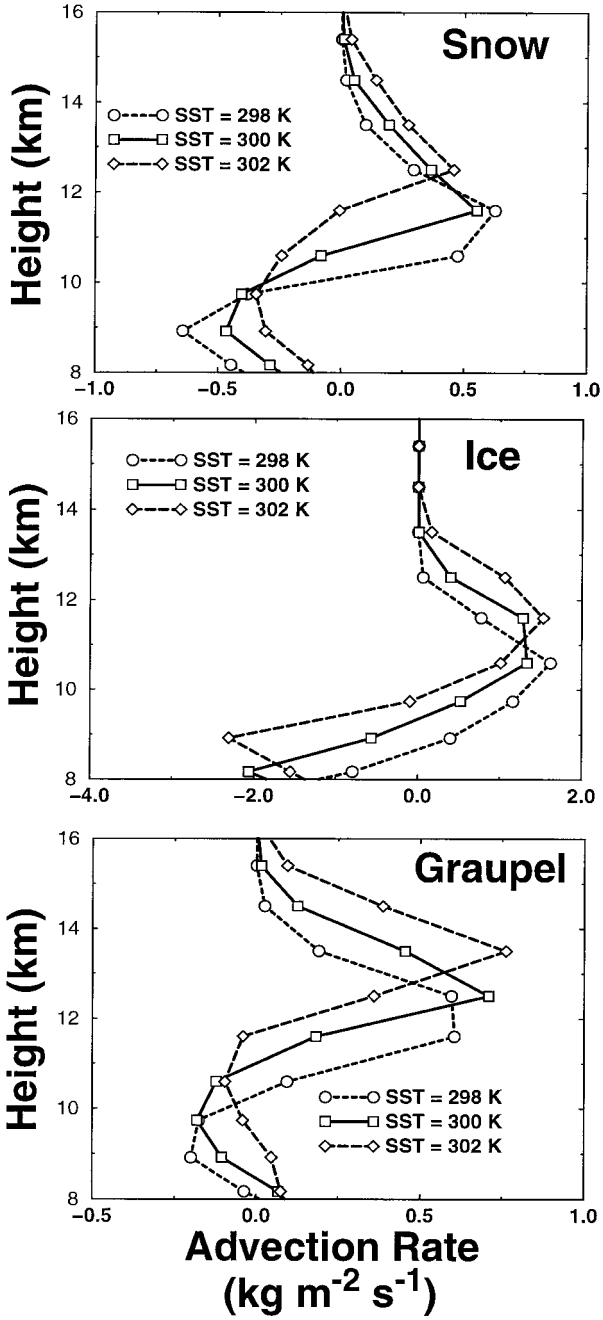

FIG. 11. Average vertical advection within all convective columns of the ice microphysical quantities of (top) snow, (middle) ice, and (bottom) graupel in the upper part of the model domain.

within the convective turrets themselves, the ''in-core'' average vertical advection terms of snow, graupel, and ice are calculated for all columns within the domain that contain at least one (up or downdraft) convective grid point (using the 1 m s^{-1} kinematic criterion as before). The calculated values (Fig. 11) do not represent total vertical flux of these quantities, since snow and graupel fall speeds are not taken into account, but indicate the convective transport of the microphysical quantities taking their mass–mixing ratios and changing vertical convective mass flux into consideration. The statistics will also be somewhat ''diluted'' by the nonconvective grid points within convectively classified columns. Only the upper-cloud region is shown since these are the heights at which the ice-category interconversation takes place.

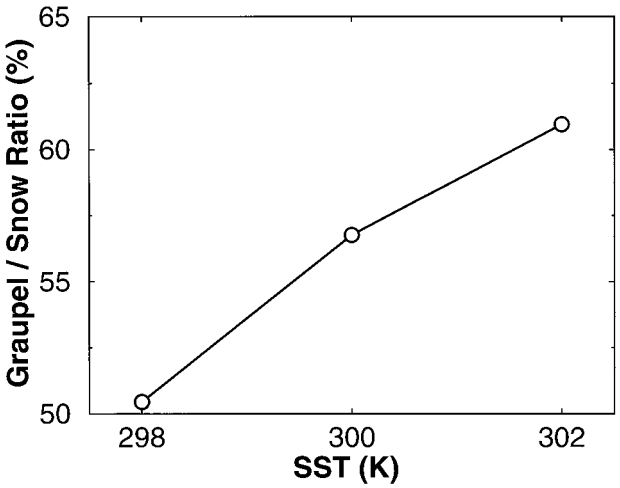

FIG. 12. Ratio of total column graupel condensate mass to that of snow.

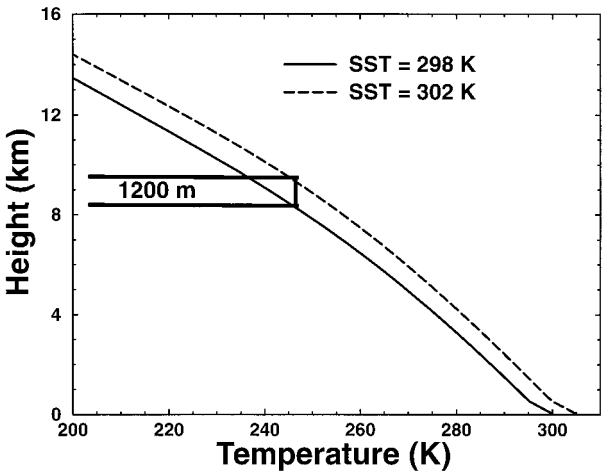

FIG. 13. Virtual temperature profiles for a reversibly lifted surface parcel (as in the calculation of CAPE) in the warm and cool SST experiments. The profile is seen to increase by 1200 m as the SST warms by 4 K.

The magnitude of ice crystal transport is found to be almost insensitive to SST changes, with the whole profile simply shifting in height. A similar pattern is observed in advective transport in nonconvective cloud (not shown). A conclusive proof of the insensitivity of the microphysical evolution of the cloud to SST would require a full budget of microphysical quantities, preferably in a Lagrangian framework following the ascending air parcels. Such an analysis may be undertaken in future work.

The most significant change with SST in cloud microphysics is evidenced in the snow and graupel panels of Fig. 11, where it is seen that graupel advection grows with increasing SST at the expense of snow. This is due to the dominant snow to graupel autoconversion process (PGAUT), parameterized by

$$\text{PGAUT} = 10^{-3} \exp[0.09(T - T_0)](q_s - q_{s0}), \quad (1)$$

as in Lin et al. (1983), where T represents the temperature, T_0 is the melting temperature of 273.15 K, q_s is the ice mass–mixing ratio, and q_{s0} is the threshold snow mass–mixing ratio for this process to occur (set here to 10^{-3} kg kg^{-1}). It is seen that the process appears to become more efficient at warmer temperatures indicating that graupel could be formed more quickly over warmer SSTs. Over the 4-K increase in SST, the ratio of total column graupel condensate mass to that snow increases from around 50% to almost 61% (Fig. 12). This could explain the drop in cloud fraction with increasing SST (section 4b), since graupel condensates have higher terminal fall velocities than snow and therefore cannot be horizontally advected as far before they fall out of the anvil region. This is also consistent with the findings of the previous section that showed increased downdraft mass fluxes in the warm run experiment. The higher fall velocities of graupel presumably lead to larger mass flux in the upper-level downdraft arising directly from the outflow of deep convective systems.

The profiles in Fig. 11 are seen to increase in height by 1200 m or so over the 4-K SST range, which matches the change in the height where any given temperature value is encountered by a parcel of air lifted moist adiabatically from the 50-m layer (Fig. 13). However, the cloud-top height increase is only 600 m, and the cloud-top temperature actually increases with increasing SST. The cloud-top height and temperature are determined by the level of zero buoyancy, where the moist adiabat of the lifted parcel intersects the radiative equilibrium temperature profile of the stratosphere. Due to the presence of stratospheric ozone, the radiative equilibrium temperature increases with height, leading to increased cloud-top temperature with increasing SST and a lower cloud top than would be obtained with an isothermal lower stratosphere. It should be noted that two feedbacks that may affect the temperature of the lower stratosphere have not been included in the simulations; the ozone profile is fixed, and wave-driven ascent is ignored.

7. Radiation feedbacks

Observational and general circulation model studies use the concept of a ''feedback parameter'' in order to assess the relative radiative importance of the various changes in atmospheric quantities such as cloud properties or water vapor amount that may occur in a future climate regime. The analysis technique assumes that the climate system is in thermodynamic and radiative equilibrium when considered over some suitable time period, which then experiences an external radiative forcing, G, (an increase in atmospheric CO_2 or a change in the solar constant for example) which is small enough to allow the climate's temperature response to be treated linearly.

Only a brief introduction will be given since the method is already comprehensively documented in Dickinson (1981), Schlesinger (1985), Schlesinger and Mitchell (1987), Cess and Potter (1988), Arking (1991), Zhang et al. (1994), and Dutton (1995), for example, albeit with varying notation.

Following Cess and Potter (1988), if F and Q represent the emitted IR and the net downwards shortwave (SW) fluxes at the top of the atmosphere, respectively, then the net upward flux at the TOA is

$$G = F - Q. \tag{2}$$

If the climate is subject to some external forcing, ΔG, such as an increase in solar activity for example, then the surface temperature response (ΔT_S) to this forcing is related by the climate sensitivity parameter λ, by

$$\Delta T_S = \lambda \Delta G. \tag{3}$$

Although the Tropics in nature are not in thermodynamic and radiative equilibrium, since heat is transported to other latitudes by the atmosphere and ocean, this analysis technique can be easily used for this CRM experiment because no large-scale heat transport is represented. Since a fixed SST is imposed, the internal feedbacks are examined using the ''reverse climate'' problem as in Cess et al. (1990) and Zhang et al. (1994), where the SST perturbation is imposed and the radiative response at the top of the model atmosphere is examined after the atmosphere has reached a new thermodynamic equilibrium.

If the earth had no atmosphere, λ would simply represent the increase in IR emission to space as the surface temperature changed in response to an external climate forcing. However the earth has an overlying ''graybody'' atmosphere that will also have a temperature response. Other atmospheric properties such as clouds and water vapor amount are also likely to change, all of which feedback to alter the surface temperature change in response to the climate forcing. To isolate the effect of each process involved, the overall atmospheric feedback in the CRM is partitioned linearly (assuming no physical interaction between the feedback effects) into the effects of changing atmospheric mean temperature, atmospheric lapse rate, atmospheric water vapor amount, and the overall effect of changing cloud properties. These are the only feedbacks that operate in the CRM.

Following Zhang et al. (1994), the surface temperature feedback (represented hereafter by α_T) is defined as the combined effect of surface and atmosphere temperature changes, assuming that the change in atmospheric temperature matches that of the underlying surface. However, the atmospheric temperature response is likely in reality to be different to that of the underlying surface. This internal feedback effect is termed the lapse rate feedback (α_L). The second feedback that is still under much debate is the feedback effect of clouds (α_C), which alter both the IR and SW outgoing longwave radiation. For example, increasing SST could alter the height of cloud tops reducing their effecting emitting temperature but may also alter cloud fraction affecting both IR and SW fluxes. The last feedback effect operating in this model is due to warmer climates possibly containing more water vapour (α_W), a greenhouse gas that amplifies the climate response.

TABLE 2. Clear-sky feedbacks in the CRM.

Feedback effect	Value (W m^{-2} K^{-1})
α_T (IR)	−4.25
α_L (IR)	−1.67
α_W (IR)	+5.07
α_T (IR) + α_L (IR) + α_W (IR)	−0.85
Total clear-sky IR feedback $[-\Delta F_{\text{clr}}/\Delta T_s]$	−1.18
α_W (SW)	−0.06
Total clear-sky SW feedback $[\Delta Q_{\text{clr}}/\Delta T_s]$	−0.26

These feedbacks are incorporated into (3) by setting

$$\lambda = -(\alpha_T + \alpha_C + \alpha_W + \alpha_L)^{-1}, \tag{4}$$

where, for example, α_W is the rate of change of the radiative forcing with respect to the surface temperature $\Delta G/\Delta T_S$ when only the water vapor profile is allowed to change and all other parameters remain fixed. If W represents the water vapor profile symbolically, then

$$\alpha_W = -\frac{\Delta G}{\Delta W}\frac{\Delta W}{\Delta T_S}. \tag{5}$$

a. Clear-sky feedbacks

To separate the effects of temperature and water vapor in the clear-sky regions the radiation scheme is run offline for a single atmospheric column using the horizontally averaged temperature and moisture clear-sky region profiles from the control case. The effect on the TOA fluxes (ΔG) of individually changing either the moisture profile, the atmospheric mean temperature, or the atmospheric temperature lapse rate for both the warm and cold runs can then be examined, giving values for each of the clear-sky feedbacks as defined above. The calculated values for the clear-sky feedbacks are shown in Table 2. Due to the nonlinear nature of radiative heating, using averaged temperature and moisture profiles will introduce some inaccuracy in the radiative fluxes (Zhang et al. 1994) and so for comparison the total clear-sky feedback factor is also shown for both the IR and SW. Some of the difference may also be due to the assumption of linearity upon which the feedback factors are based. Since three experiments were performed, however, it was also possible to make an estimate for the second-order feedback term, and it was found that all the clear-sky feedbacks had negligibly small second-order terms.

To aid the comparison of the clear-sky feedbacks with other sources the simple model of Webb et al. (1993) is adopted that treats the atmosphere as a single non-

scattering graybody slab of emissivity ε and temperature T_A. The TOA outgoing IR flux in this model is [Webb et al. 1993, Eq. (4)]

$$F = \varepsilon\sigma T_A^4 + (1 - \varepsilon)\sigma T_S^4. \quad (6)$$

Webb et al. (1993) assume that ε is roughly proportional to atmospheric water vapor amounts that would imply a higher emissivity for the tropical atmosphere than the global average.

1) TEMPERATURE FEEDBACK

As one would expect, the negative temperature feedback ($\alpha_T = -4.25$ W m^{-2} K^{-1}) in Table 2 is very similar in magnitude to the GCM values found by Zhang et al. (1994). However, the balance between sensitivity to surface and atmospheric temperature changes in the CRM is different to the global average due to the higher atmospheric emissivity and the corresponding higher sensitivity to atmospheric temperature changes.

2) WATER VAPOR FEEDBACK

The clear-sky water vapor is a relatively large positive feedback ($\alpha_W = +5.07$ W m^{-2} K^{-1}). In observations the tropical clear-sky regions can be locally unstable, since as the SST increases, the increase in water vapor is sufficiently large to reduce outgoing IR flux; known as the supergreenhouse effect. But in order for this to happen increases in water vapor substantially in excess of the those predicted by constant relative humidity are required for the vapor effect to dominate the increasing temperature (Hallberg and Inamdar 1993). Since in the CRM the relative humidity is approximately constant, the reduction in outgoing longwave radiation is more than offset by changing atmospheric temperature.

3) LAPSE RATE FEEDBACK

The lapse rate feedback is a negative feedback in this model ($\alpha_L = -1.67$ W m^{-2} K^{-1}) since the potential temperature lapse rate increases with SST due to the approximately moist adiabatic profile that convection imposes on the tropical atmosphere. Proportionally the lapse rate feedback is much higher relative to the water vapor feedback than in observational tropical studies (e.g., Weaver et al. 1994), probably because of the smaller changes in water vapor. The feedback could also be greater in magnitude than GCM-derived values for the global atmosphere for a number of reasons: the higher atmospheric emissivity in the Tropics; the moist adiabatic temperature profile in the Tropics could exhibit greater changes in static stability than will occur at higher latitudes; and the redistribution of atmospheric heat by the large-scale circulation from high to low SST regions within the Tropics would reduce the sensitivity in a GCM.

In summary, the clear-sky temperature feedback response of the CRM is roughly similar to observational studies in terms of temperature changes since the atmospheric temperature profile is tightly controlled by the underlying SST and the moist adiabatic structure imposed by convection. However, without enhancement of convective activity by the large-scale flow, the temperature and vapor changes to a large extent cancel each other. Thus the conclusion can be made that the observed tropical supergreenhouse effect, resulting from large increases in atmospheric water vapor, is the result of large-scale dynamics resulting from SST gradients rather than a local convective response to increasing SSTs, and is entirely consistent with the earlier findings of Sui et al. (1993) and Lau et al. (1994).

TABLE 3. Cloud feedbacks in the CRM.

Feedback effect	Value (W m^{-2} K^{-1})
α_C (IR)	−0.56
α_C (SW)	+0.49
Total cloudy-sky feedback [α_C (IR) + α_C (SW)]	−0.07

b. Cloud feedback

To examine the total cloud feedback effect, the common method of separating G into its clear and cloudy sky components is used by calculating the cloud radiative forcing (CRF; e.g., Cess et al. 1990; Senior and Mitchell 1993; Collins et al. 1996):

$$\text{CRF} = G_{\text{clr}} - G, \quad (7)$$

where G_{clr} represents the net upward radiative flux at the TOA for the clear-sky regions only. Since clouds do not affect the clear regions (due to the assumption of the two-stream approximation), then it is straightforward to show that

$$\alpha_C = \frac{\Delta\text{CRF}}{\Delta T_s} \quad (8)$$

$$\alpha_W + \alpha_L + \alpha_T = \frac{-\Delta G_{\text{clr}}}{\Delta T_s}. \quad (9)$$

Thus the difference between the clear and cloudy-sky TOA fluxes in the cloud model gives the cloud feedback, which is summarized in Table 3. As noted by Zhang et al. (1994), using this method means that the cloud feedback factor includes the feedback due to differing water vapor and temperature profiles that exist in the cloudy regions compared to the clear-sky regions in addition to the direct effect of clouds themselves on the radiation budgets.

The cloud feedback in the infrared is a small negative feedback since as the SST increases the cloud warms the atmosphere slightly less. Although the cloud-top heights are increasing with SST, the atmospheric temperature increased more rapidly resulting in increased cloud-top temperatures. Additionally the decreasing

cloud fraction also acts to reduce cloud warming. In contrast, clouds in the shortwave act as a small positive feedback since the decreasing cloud-fraction results in less shortwave radiation being reflected back to space. Both of these effects of clouds are small when compared to the clear-sky feedbacks.

Since the action of clouds in the shortwave and infrared spectra cancels, the net effect of clouds (α_C) is a negligibly small negative feedback in this model ($\alpha_C = -0.07$ W m^{-2} K^{-1}). In observational studies using satellite data such as Ramanathan et al. (1989) and Kiehl (1994) short- and longwave cloud forcing are found to almost cancel over a wide range of cloud conditions. This cancellation has even been found to hold over the space and timescales of a single cloud system using in situ measurements (Collins et al. 1996). A zero net CRF in today's climate does not necessarily imply a zero cloud feedback factor though, since it is the change in CRF that determines the feedback effect of clouds. However, since cloud properties change very little with SST in the CRM, the cloud feedback indeed turns out to be very small in magnitude.

In GCM studies the spread of assessed cloud feedback factors has been considerable (Cess et al. 1990), including both negative and positive feedbacks. It is interesting to note that in a more recent GCM intercomparison (Cess et al. 1996) the cloud feedback factors were more in agreement with each other and more negative in magnitude, although this is not necessarily attributable to improvements in cloud parameterization schemes in the GCMs.

An examination of the second-order terms shows that the infrared cloud feedback factor was significantly nonlinear with a second-order term of 0.22 W m^{-2} K^{-2}. Although it is not possible to make firm statements concerning the nonlinearity of cloud properties with only three experiments, this does highlight a possible danger of assuming linear process responses in GCM experiments, which are often conducted at only two SSTs, and possibly advocates the use in certain circumstances of feedback analysis models that easily incorporate higher-order terms such as in Tompkins (1997).

8. Summary and discussion

In their examination of the role of the large-scale circulation in the relationship between tropical convection and SST using observational data, Lau et al. (1997) reached the conclusion that the sensitivity of convection to changing SST was greatly reduced in the absence of large-scale flow. They note however, the difficulty in isolating unambiguously in data one effect (large-scale flow) from two others (changing SST and convective activity) when a three-way coupling between the three exists and conclude that ''clearly the results . . . should be tested with numerical models.'' The cloud resolving model is an ideal tool for performing these tests, since, by running a cloud resolving model with interactive radiative heating and a representation of convective cloud microphysics to an equilibrium state over a range of ocean temperatures, the changing characteristics of convection with SST can be analyzed where hopefully a good representation of many of the relevant local-scale interactions are included (convective dynamics–radiation–surface fluxes), but where the effects of large-scale flow are absent.

Sui et al. (1993) and Lau et al. (1994) used such a two-dimensional model to indicate that convection is indeed relatively insensitive to the underlying SST. In this paper the aim was to test the observational results with a three-dimensional cloud model and focus more on the sensitivity of the microphysical processes. Three experiments were performed, with an equilibrium achieved for SSTs of 298, 300, and 302 K, a temperature range usually associated with a drastic change in convective activity in the Tropics.

The results can be summarized as follows: the temperature structure changes as one would expect assuming a moist adiabatic structure, the moisture increase is consistent throughout most of the troposphere with the assumption of constant relative humidity, and in terms of convective mass fluxes, moisture transport, and cloud cover the convective activity exhibits virtually no significant changes at all; entirely consistent with both the earlier numerical studies of Sui et al. (1993) and Lau et al. (1994), and the observational studies of Lau et al. (1997) and Bony et al. (1997). In the first instance this is perhaps surprising since the microphysical scheme in the model contains a web of 37 terms for conversion of water substance between the various bulk categories, some of which are hugely temperature sensitive, exhibiting an order of magnitude change in conversion rate over the temperature range investigated here. The reason this does not impact on the cloud properties as SST increases is due to the moist adiabatic profile the vertical temperature structure is constrained to take. A parcel undergoing ascent through a deep convective cloud experiences approximately the same range of temperatures over higher SST oceans, but simply at a higher altitude. This means that the cloud properties and radiative forcings are therefore relatively insensitive to changes in SST.

This is not to state, however, that cloud microphysics is not an important issue. The structure of the clouds—and the entire equilibrium state properties such as water vapor, profile, and convective mass flux distribution between up and down draughts—will be crucially sensitive to the microphysical parameterization, which is why convective parameterization schemes such as Emanuel (1991) have started to attempt to include at least a rudimentary representation of microphysical processes. It is supposed that differing microphysical parameterization schemes are responsible for some of the differences between CRM studies such as Grabowski et al. (1996) and Sui et al. (1994), which produced starkly contrasting equilibrium states for similar experimental setups. This

is one aspect of cloud modeling that should be addressed in cloud intercomparison studies such as the Global Energy and Water Cycle Experiment cloud system study (Moncrieff et al. 1997), which will hopefully produce more consensus between future CRMs and lead to improved cloud schemes in GCMs. It should be noted, for example, that the microphysical scheme used in the experiments in this paper rendered comparatively small cloud anvil coverage. It may be that an alternative scheme that is more prolific in producing anvil cloud could show a larger sensitivity to atmospheric temperatures.

That said, a comfortable conclusion from this study is that, in the Tropics at least, if a cloud parameterization scheme involving microphysical processes could be developed that represented today's cloud climatology in all its forms reasonably well, then it is possible to have a reasonable level of confidence that it will represent changes in cloud properties well in future climate scenarios, *providing any warming in that climate acts uniformly to first order.* This last cautionary stipulation is added since, if a future climate exhibited large changes in horizontal surface temperature gradients, the influence of the large-scale flow could greatly amplify the effect of the microphysical sensitivities of convection. In this study, for example, the graupel category of ice condensate increased in importance (nonlinearly) at the expense of the snow phase, resulting in falling cloud fractions as the SST increased. Large-scale flow alterations could greatly exacerbate this, both by forcing increased mass fluxes and by altering convective organisation via the action of vertical wind shear, for example.

It is left to future work to directly investigate the role of the large-scale flow in a cloud resolving model framework. This could take the form, for example, of a cloud resolving study conducted with a domain of large horizontal extent in one direction with an underlying SST gradient representative of the equatorial Pacific Ocean, but also with a limited third dimension (of say, 100 km) that would allow convection to adopt realistic three dimensional geometry. Such domain sizes are now becoming feasible with the advent of parallel computing resources. The effect of uniform SST increases and changing SST gradients could then be investigated.

Acknowledgments. We thank the U.K. Meteorological Office for supplying both the cloud resolving model and radiation code used in this study. Dr. C. H. Sui and an anonymous reviewer made many helpful suggestions to improve the original manuscript. Prof. K.-M. Lau and Dr. C. H. Sui are thanked for informing us of some earlier work we were previously unaware of. Tristan Guillot is also thanked for helpful discussions on this subject, and many useful comments were received from Mike Blackburn who reviewed an early version of the manuscript. Adrian Tompkins was supported by NERC during this study.

REFERENCES

Arking, A., 1991: The radiative effects of clouds and their impact on climate. *Bull. Amer. Meteor. Soc.,* **72,** 795–813.

——, and D. Ziskin, 1994: Relationship between clouds and sea surface temperature in the western tropical Pacific. *J. Climate,* **7,** 988–1000.

Betts, A. K., 1990: Greenhouse warming and the tropical water budget. *Bull. Amer. Meteor. Soc.,* **71,** 1464–1465.

Bony, S., K.-M. Lau, and Y. C. Sud, 1997: Sea surface temperature and large-scale circulation influences on tropical greenhouse effect and cloud radiative forcing. *J. Climate,* **10,** 2055–2076.

Bretherton, C. S., and P. K. Smolarkiewicz, 1989: Gravity waves, compensating subsidence and detrainment around cumulus clouds. *J. Atmos. Sci.,* **46,** 740–759.

Brown, P. R. A., and H. A. Swann, 1997: Evaluation of key microphysical parameters in three dimensional cloud model simulations using aircraft and multiparameter radar data. *Quart. J. Roy. Meteor. Soc.,* **123,** 2245–2275.

Cess, R. D., and G. L. Potter, 1988: A methodology for understanding and intercomparing atmospheric climate feedback processes in general circulation models. *J. Geophys. Res.,* **93,** 8305–8314.

——, and Coauthors, 1990: Intercomparison of climate feedback processes in 19 atmospheric general circulation models. *J. Geophys. Res.,* **95,** 16 601–16 615.

——, and Coauthors, 1996: Cloud feedback in atmospheric general circulation models: An update. *J. Geophys. Res.,* **101,** 12 791–12 794.

Collins, W. D., F. P. J. Valero, P. J. Flatau, D. Lubin, H. Grassl, and P. Pilewskie, 1996: Radiative effects of convection in the tropical Pacific. *J. Geophys. Res.,* **101,** 14 999–15 012.

Dickinson, R. E., 1981: Convergence rate and stability of ocean–atmosphere coupling schemes with a zero-dimensional climate model. *J. Atmos. Sci.,* **38,** 2112–2120.

——, V. Meleshko, D. Randall, E. Sarachik, P. Silva-Dias, and A. Slingo, 1996: Climate processes. *Climate Change 1995: The Science of Climate Change,* J. T. Houghton, L. G. Meira Filho, B. A. Callander, N. Harris, A. Kattenberg, and K. Maskell, Eds., Cambridge University Press, 193–227.

Dutton, J. A., 1995: An analytical model of atmospheric feedback and global temperature change. *J. Climate,* **8,** 1122–1139.

Duvel, J. P., and F. M. Bréon, 1991: The clear-sky greenhouse effect sensitivity to a sea surface temperature change. *J. Climate,* **4,** 1162–1169.

Edwards, J. M., and A. Slingo, 1996: Studies with a flexible new radiation code. Part I: Choosing a configuration for a large-scale model. *Quart. J. Roy. Meteor. Soc.,* **122,** 689–719.

Emanuel, K. A., 1991: A scheme for representing cumulus convection in large-scale models. *J. Atmos. Sci.,* **48,** 2313–2335.

——, 1996: Convective cloud microphysics and climate change. Preprints, *Seventh Conf. on Mesoscale Processes,* Reading, United Kingdom, Amer. Meteor. Soc., 615–617.

——, J. D. Neelin, and C. S. Bretherton, 1994: On large-scale circulations in convecting atmospheres. *Quart. J. Roy. Meteor. Soc.,* **120,** 1111–1143.

Fu, R., A. D. Del Genio, and W. B. Rossow, 1990: Behavior of deep convective clouds in the tropical Pacific deduced from ISCCP radiances. *J. Climate,* **3,** 1129–1152.

——, ——, and ——, 1994: Influence of ocean surface conditions on atmospheric vertical thermodynamic structure and deep convection. *J. Climate,* **7,** 1092–1108.

Gaffen, D. J., W. P. Elliot, and A. Robock, 1992: Relationships between tropospheric water vapor and surface temperature as observed by radiosondes. *Geophys. Res. Lett.,* **19,** 1839–1842.

Garratt, J. R., 1992: *The Atmospheric Boundary Layer.* Cambridge University Press, 316 pp.

Grabowski, W. W., M. W. Moncrieff, and J. T. Kiehl, 1996: Long-term behaviour of precipitating tropical cloud systems: A numerical study. *Quart. J. Roy. Meteor. Soc.,* **122,** 1019–1042.

Graham, N. E., and T. P. Barnett, 1987: Sea surface temperature,

surface wind divergence, and convection over the tropical oceans. *Science,* **238,** 657–659.
Hallberg, R., and A. K. Inamdar, 1993: Observations of seasonal variations in atmospheric greenhouse trapping and its enhancement at high sea surface temperature. *J. Climate,* **6,** 920–931.
Held, I. M., R. S. Hemler, and V. Ramaswamy, 1993: Radiative-convective equilibrium with explicit two-dimensional moist convection. *J. Atmos. Sci.,* **50,** 3909–3927.
Jorgensen, D. P., and M. A. Lemone, 1989: Vertical velocity characteristics of oceanic convection. *J. Atmos. Sci.,* **46,** 621–640.
Kiehl, J. T., 1994: On the observed near cancellation between longwave and shortwave cloud forcing in tropical regions. *J. Climate,* **7,** 559–565.
Kuo, H. L., 1974: Further studies of the parameterization of the influence of cumulus convection on large-scale flow. *J. Atmos. Sci.,* **31,** 1232–1240.
Lau, K.-M., C. H. Sui, and W. K. Tao, 1993: A preliminary study of the tropical water cycle and its sensitivity to surface warming. *Bull. Amer. Meteor. Soc.,* **74,** 1313–1321.
——, ——, M. D. Chou, and W. K. Tao, 1994: An inquiry into the cirrus-cloud thermostat effect for tropical sea surface temperature. *Geophys. Res. Lett.,* **21,** 1157–1160.
——, H.-T. Wu, and S. Bony, 1997: The role of large-scale atmospheric circulation in the relationship between tropical convection and sea surface temperature. *J. Climate,* **10,** 381–392.
LeMone, M. A., and E. J. Zipser, 1980: Cumulonimbus vertical velocity events in GATE. Part I: Diameter, intensity and mass flux. *J. Atmos. Sci.,* **37,** 2444–2457.
Leonard, B. P., 1991: The ULTIMATE conservative difference scheme applied to unsteady one-dimensional advection. *Comput. Methods Appl. Mech. Eng.,* **19,** 17–74.
Lin, Y.-L., R. D. Farley, and H. D. Orville, 1983: Bulk parameterization of the snow field in a cloud model. *J. Climate Appl. Meteor.,* **22,** 1065–1092.
Lucas, C., E. J. Zipser, and M. A. Lemone, 1994: Vertical velocity in oceanic convection off tropical Australia. *J. Atmos. Sci.,* **51,** 3183–3193.
Moncrieff, M. W., S. K. Krueger, D. Gregory, J. L. Redelsperger, and W.-K. Tao, 1997: GEWEX Cloud System Study (GCSS) Working Group 4: Precipitating convective cloud systems. *Bull. Amer. Meteor. Soc.,* **78,** 831–845.
Petch, J., 1995: Modelling the interaction of clouds and radiation using bulk microphysical schemes. Ph.D. thesis, University of Reading, 191 pp.
——, 1998: Improved radiative transfer calculations from information provided by bulk microphysical schemes. *J. Atmos. Sci.,* **55,** 1846–1858.
Ramanathan, V., and W. Collins, 1991: Thermodynamic regulation of ocean warming by cirrus clouds deduced from observations of the 1987 El Nino. *Nature,* **351,** 27–32.
——, R. D. Cess, E. F. Harrison, P. Minnis, B. R. Barkstrom, E. Ahmad, and D. Hartmann, 1989: Cloud-radiative forcing and climate: Results from the earth radiation budget experiment. *Science,* **243,** 57–63.
Raval, A., and V. Ramanathan, 1989: Observational determination of the greenhouse effect. *Nature,* **342,** 758–761.
Robe, F. R., and K. A. Emanuel, 1996: Dependence of tropical convection on radiative forcing. *J. Atmos. Sci.,* **53,** 3265–3275.
Schlesinger, M. E., 1985: Feedback analysis of results from energy balance and radiative-convective models. *Projecting the Climatic Effects of Increasing Carbon Dioxide,* M. C. MacCracken and F. M. Luther, Eds., U.S. Department of Energy, 280–319.
——, and J. F. B. Mitchell, 1987: Climate model simulations of the equilibrium climatic response to increased carbon dioxide. *Rev. Geophys.,* **25,** 760–798.
Senior, C. A., and J. F. B. Mitchell, 1993: Carbon dioxide and climate: The impact of cloud parameterization. *J. Climate,* **6,** 393–418.
Shine, K. P., and A. Sinha, 1991: Sensitivity of the Earth's climate to height-dependent changes in the water vapour mixing ratio. *Nature,* **354,** 382–384.
Shutts, G. J., and M. E. B. Gray, 1994: A numerical modelling study of the geostrophic adjustment following deep convection. *Quart. J. Roy. Meteor. Soc.,* **120,** 1145–1178.
Stephens, G. L., 1990: On the relationship between water vapor over the oceans and sea surface temperature. *J. Climate,* **3,** 634–645.
Sui, C. H., K. M. Lau, W. K. Tao, M. D. Chou, and J. Simpson, 1993: Simulated water and radiation budgets in the Tropics. Preprints, *20th Conf. on Hurricanes and Tropical Meteorology,* San Antonio, TX, Amer. Meteor. Soc., 431–434.
——, ——, ——, and J. Simpson, 1994: The tropical water and energy cycles in a cumulus ensemble model. Part I: Equilibrium climate. *J. Atmos. Sci.,* **51,** 711–728.
Sun, D. Z., and R. S. Lindzen, 1993: Distribution of tropical tropospheric water vapor. *J. Atmos. Sci.,* **50,** 1643–1660.
Swann, H., 1994: Cloud microphysical processes—A description of the parameterization used in the Large Eddy Model. JCMM Internal Rep. 10, 22 pp. [Available from Joint Centre for Mesoscale Meteorology, University of Reading, P.O. Box 243, Earley Gate, Reading RG6 6BB, United Kingdom.]
Taylor, J. P., J. M. Edwards, M. D. Glew, P. Hignett, and A. Slingo, 1996: Studies with a flexible new radiation code. Part II: Comparisons with aircraft shortwave data. *Quart. J. Roy. Meteor. Soc.,* **122,** 839–861.
Tiedtke, M., 1989: A comprehensive mass flux scheme for cumulus parameterization in large-scale models. *Mon. Wea. Rev.,* **117,** 1779–1800.
Tompkins, A. M., 1997: Radiative-convective equilibrium of the tropical troposphere. Ph.D. thesis, University of Reading, 158 pp.
——, and G. C. Craig, 1998a: Radiative-convective equilibrium in a three-dimensional cloud ensemble model. *Quart. J. Roy. Meteor. Soc.,* **124,** 2073–2097.
——, and ——, 1998b: Timescales of adjustment to radiative-convective equilibrium in the tropical atmosphere. *Quart. J. Roy. Meteor. Soc.,* **124,** 2693–2713.
Waliser, D. E., and N. E. Graham, 1993: Convective cloud systems and warm-pool sea surface temperatures: Coupled interactions and self-regulation. *J. Geophys. Res.,* **98,** 12 881–12 893.
Weaver, C. P., W. D. Collins, and H. Grassl, 1994: Relationship between clear-sky atmospheric greenhouse effect and deep convection during the Central Equatorial Pacific Experiment: Model calculations and satellite observations. *J. Geophys. Res.,* **99,** 25 891–25 901.
Webb, M. J., A. Slingo, and G. L. Stephens, 1993: Seasonal variations of the clear-sky greenhouse effect: The role of changes in atmospheric temperatures and humidities. *Climate Dyn.,* **9,** 117–129.
Xu, K.-M., and D. A. Randall, 1995: Impact of interactive radiative transfer on the macroscopic behaviour of cumulus emsembles. Part I: Radiation parameterization and sensitivity tests. *J. Atmos. Sci.,* **52,** 785–799.
——, and ——, 1997: Statistical-equilibrium states of radiative-convective systems over the tropical oceans. Preprints, *22d Conf. on Hurricanes and Tropical Meteorology,* Fort Collins, CO, Amer. Meteor. Soc., 67–68.
Zhang, C., 1993: Large-scale variability of atmospheric deep convection in relation to sea surface temperature in the tropics. *J. Climate,* **6,** 1898–1913.
Zhang, M. H., J. J. Hack, J. T. Kiehl, and R. D. Cess, 1994: Diagnostic study of climate feedback processes in atmospheric general circulation models. *J. Geophys. Res.,* **99,** 5525–5537.